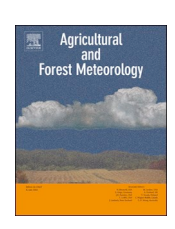
FISEVIER

Contents lists available at ScienceDirect

Agricultural and Forest Meteorology

journal homepage: www.elsevier.com/locate/agrformet



Research Paper

Impact of tidal inundation on the net ecosystem exchange in daytime conditions in a salt marsh



H. Nahrawi^{a,b,*}, M.Y. Leclerc^a, S. Pennings^c, G. Zhang^a, N. Singh^a, R. Pahari^a

- ^a Atmospheric Biogeosciences Group, Department of Crop and Soil Sciences, The University of Georgia, Griffin, GA, 30223, USA
- ^b Faculty of Resource Science and Technology, Universiti Malaysia Sarawak, 94300, Malaysia
- ^c Department of Biology and Biochemistry, University of Houston, Houston, TX, 77204, USA

ARTICLE INFO

Keywords: Eddy-covariance CO₂ exchange Net ecosystem exchange Tidal inundation Spartina alterniflora Salt marsh

ABSTRACT

Salt marshes are highly productive ecosystems and yet we have only a preliminary understanding of how net ecosystem exchange varies on daily and seasonal time scales. We used the eddy-covariance method to examine the behaviour of the net ecosystem exchange as influenced by tidal flooding in daytime conditions in a coastal salt marsh dominated by *Spartina alterniflora* in Georgia, USA. Two different analyses both found that the net ecosystem exchange was $\sim 60\%$ greater during neap high tides than during spring high tides; the largest differences occurred early in the growing season. The effect of tidal flooding varied continuously with the degree to which plants were inundated versus emergent. The total monthly reduction (less negative) in daytime net ecosystem exchange due to flooding was 7-38% and 1-64% in 2014 and 2015 respectively. The highest CO_2 flux reductions were observed early and during the peak growing season (February, March, April and May) and the lowest during the summer season in both years. Our findings suggest that daytime CO_2 flux was reduced (less negative) 20-60% during the peak growing season due to tidal flooding. A better understanding of the impact of seasonal tidal flooding on net ecosystem exchange may allow more sophisticated predictions of how sea level rise will affect marsh function and survival over the coming century.

1. Introduction

Coastal salt marshes are among the most productive ecosystems on earth, sequestering an average of 210 g C m $^{-2}$ yr $^{-1}$ (Cai, 2011; Chmura et al., 2003; Duarte et al., 2005). They occur in the intertidal zone where they are alternately flooded by the ocean and exposed. Tides also play an important role in the lateral exchange of matter, importing inorganic nutrients into marshes and exporting organic nutrients from marshes (Wang et al., 2018). The depth of marsh flooding varies with the lunar cycle, with spring tides flooding the intertidal to a greater depth than neap tides. The depth of tidal flooding is also affected by sea level. Sea level is rising globally by several mm/y (Morris et al., 2013). Understanding how salt marshes respond to inundation is therefore essential to both understanding and forecasting the productivity of these vital ecosystems.

Although a number of studies have examined net ecosystem exchange in salt marsh ecosystems (Forbrich and Giblin, 2015; Guo et al., 2009; Kathilankal et al., 2008; Moffett et al., 2010), we still have only a preliminary understanding of how CO₂ exchange is affected by tidal flooding. Studies using closed chambers have typically found that tidal

flooding decreased CO_2 fluxes (less negative) (Yamamoto et al. 2009, Tong et al. 2013). A study using the eddy-covariance method suggested that the CO_2 flux was more sensitive to tidal flooding at a low versus a high elevation site (Guo et al. 2009). With eddy-covariance measurements, Schedlbauer et al. (2010) reported that net ecosystem exchange and ecosystem respiration of a short-hydroperiod fresh-water marl marsh in the Everglades, Florida, decreased in the wet season compared to the dry season and that macrophyte CO_2 uptake was also reduced during inundation. Intensified inundation can shift a freshwater wetland from a CO_2 sink to a source, as ecosystem respiration is less responsive to intensified inundation than gross primary production (Zhao et al. 2019). How tidal flooding alters the exchange of CO_2 on a monthly time scale, and how this effect varies seasonally, remains to be explored.

We used the eddy-covariance method to measure the impact of tidal flooding on net ecosystem exchange (hereafter, NEE) in daytime conditions in a salt marsh on the southeast coast of North America dominated by the grass *Spartina alterniflora* Loisel (species *Smooth Cordgrass*). *S. alterniflora* forms extensive monospecific stands in intertidal environments. We hypothesized that daytime CO₂ exchange in the salt

E-mail address: nhafsah@unimas.my (H. Nahrawi).

^{*} Corresponding author.

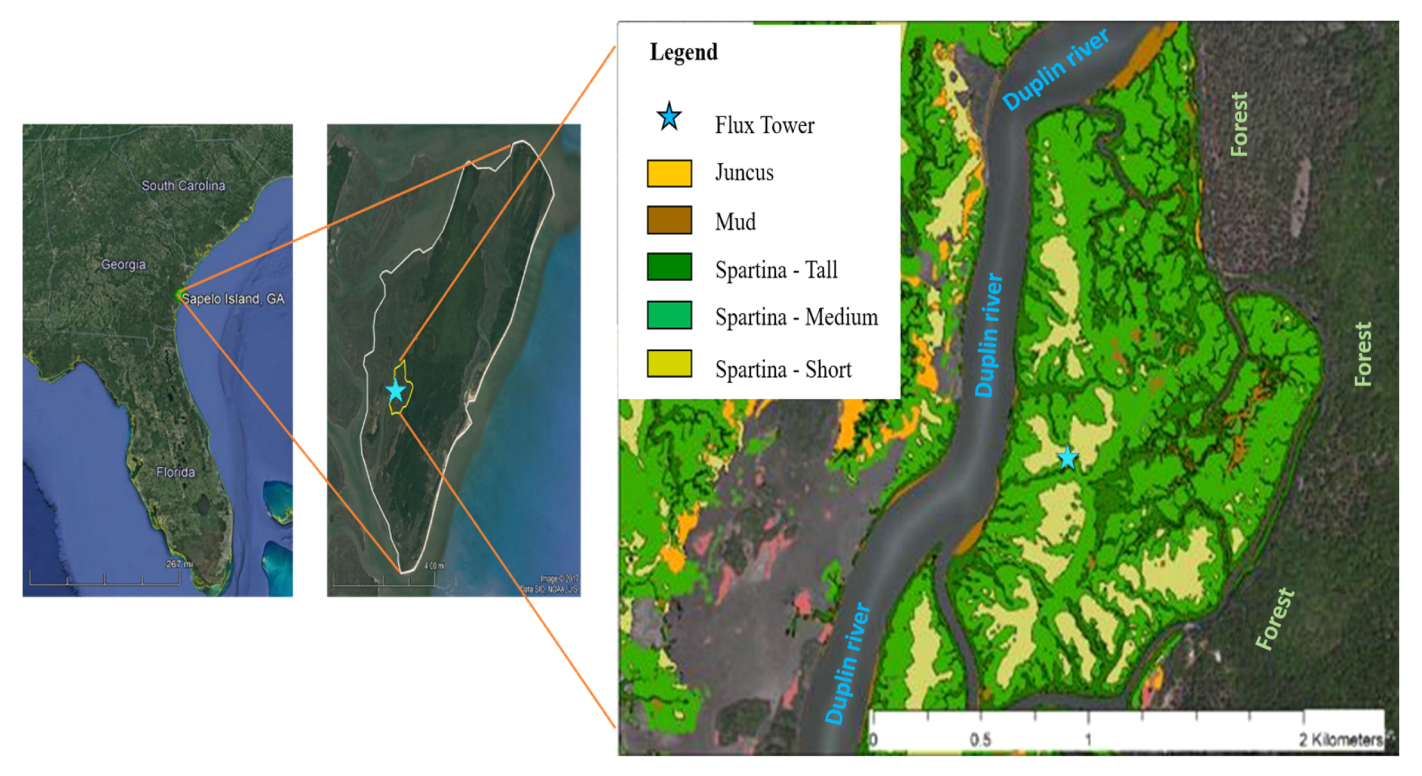


Fig. 1. Study site at Sapelo Island, Georgia, USA. Left: The location of Sapelo Island on the southeast coast of the United States (Google Earth Image). Middle: Sapelo Island (Google Earth Image). Right: Close-up of the location of the study site area with different height forms of Spartina alterniflora indicated by different colors and with Duplin river on the west side and forest on the east side of the flux tower also labeled. Blue stars in both images indicate the location of flux tower (Image courtesy: Christine Hladik, GCE LTER).

marsh would be related to 1) the amount of vegetation exposed to the atmosphere, 2) light intensity, and 3) the seasonal growth cycle of the plant. Our objectives were (i) to determine the effect of daily and seasonal cycles of tidal inundation on CO_2 exchange between the marsh and the atmosphere; and (ii) to quantify the total monthly reduction of daytime CO_2 exchange between the salt marsh and atmosphere as a result of tidal inundation.

2. Materials and methods

2.1. Study site

We worked at the Georgia Coastal Ecosystem Long-Term Ecological Research (GCE-LTER) site near Sapelo Island, GA (Latitude: 31.441°, Longitude: 81.284°). The study site is heterogeneous and surrounded by other ecosystems such as the Duplin River to the West and a forest to the East (Figure 1). The site experiences semi-diurnal tides with a mean tide of 2.5 m (Chalmers, 1997). Water column salinities typically range from 25 to 35 PSU. The site is dominated by approximately 40 ha of smooth cordgrass, S. alterniflora (Bortolus et al., 2019), which is physiologically adapted to anoxic and high salinity conditions typical of salt marsh ecosystems. S. alterniflora varies in height from ~ 0.1 m in stressful habitats to ~ 2.0 m close to the tidal creeks and channels (Richards et al., 2010). At high tide, short S. alterniflora plants can be completely submerged by the tide, while tall S. alterniflora plants are usually still partly exposed to the atmosphere. The combination of both tidal inundation and the complex mosaic of S. alterniflora patches of varying heights is challenging for rigorous signal processing and subsequent interpretation of the eddy-covariance technique data. The latter is predicated on the idea that the flux measurements is representative of an upwind region of uniform properties, hence the concept of footprint.

Spartina alterniflora at the site grows rapidly from late February to the middle of July. Maximum biomass peaks during the months of May

through July. *S. alterniflora* plants senescence between September and late November, with minimum levels of live biomass present between late November and late February (O'Connell et al., 2019).

2.2. Climatological conditions

We report on data collected between January 2014 to December 2015. Annual mean air temperature (Tair) in 2014 and 2015 was approximately 0.4°C below and 1.1°C higher than the long-term average (2003-2016) (NOAA, 2016), respectively, with 2015 being one of the warmest years since 1998 (US EPA, 2016). Seasonal trends of soil temperature (T_{soil}) followed a similar pattern to that of T_{air}. The annual mean of photosynthetic active radiation (PAR) was higher in 2014 than 2015. The annual precipitation in 2014 (1296 mm) was slightly higher than the long-term (2003-2016) average of 1227 mm and exceeded the annual precipitation in 2015 (1050 mm) by 19%. Total precipitation varied markedly between seasons, with precipitation peaking during the summer months. The prevailing wind during 2014 and 2015 was predominantly northeasterly in winter, south and southeasterly in spring, and south and southwesterly in summer. The prevailing wind direction during the fall was mostly southeasterly in 2014 and northeasterly in 2015. The data were screened based on the prevailing wind direction as described in sub-Section 2.4.1.

2.3. Field measurements

2.3.1. Eddy-covariance

We collected data from two eddy-covariance (EC) systems installed on a flux tower at the head of a small tidal creek on the Duplin River (Fig. A.1). The systems were mounted 5 m above the ground facing South (180°, hereafter south system) and North (0°, hereafter north system). Five meter was selected, considering Spartina plant height, tide height, and the available fetch of the studied Spartina area. Each

system consisted of a fast-response omnidirectional 3-D sonic anemometer (CSAT3, Campbell Scientific Inc., Logan, UT, USA) to measure the three-wind components and virtual air temperature, and a closed-path $\rm CO_2/H_2O$ gas analyzer (Li-7200, Li-Cor Biosciences, Lincoln, NE, USA) to measure the atmospheric concentration of $\rm CO_2$ and $\rm H_2O$. In the closed path eddy-covariance system, air was drawn from the inlet, displaced 0.1 m laterally and 0.1 m below the center of the sonic anemometer transducers. The tubes from the inlet to the Li-7200 sensor were approximately 1 m long with an inner diameter of 4.8 mm. The pump flow was approximately 15 l min $^{-1}$. The gas analyzers were calibrated with zero and span (364.4 ppm $\rm CO_2$ and Li-Cor Li-610 dew point generator) gases every six months. During each calibration, the internal chemicals of the gas analyzers were replaced, and optical paths were cleaned. Measurements were recorded at 10Hz.

A weather station adjacent to the tower measured air temperature and relative humidity (HMP45C/HMP155, Campbell Scientific Inc., Logan, UT, USA), net radiation (CNR2 Campbell Scientific Inc., Logan, UT, USA), photosynthetic active radiation (quantum sensor LI190SB, Campbell Scientific Inc., Logan, UT, USA) and precipitation (rain gage TE525WS, Campbell Scientific Inc., Logan, UT, USA). Tidal cycles were measured with a water pressure transducer (CS455, Campbell Scientific Inc., Logan, UT, USA) installed in the creek.

2.3.2. Vegetation measurements

To document seasonal variation in vegetation height, we sampled permanent plots established in stands of *S. alterniflora* approximately 0.65 km from the flux tower. We deployed six replicate plots in short, medium and tall height forms of *S. alterniflora*, and measured the height of each stem in each plot monthly from January 2014 to December 2015 (Pennings, 2016).

2.4. Signal processing and data analysis

We screened the 10 Hz wind velocity and CO2 and H2O data for abnormal automatic gain control (AGC) and then processed the data using EddyPro 6.1 software into 30-minute blocks of CO2 and H2O flux data. We removed spikes in the signal using the method outlined in Vickers and Mahrt (1997). We applied the planar-fit method (Wilczak et al., 2001) for tilt correction due to misalignment of the sonic anemometer with the local wind. We checked for linear trends in 10-Hz time series of each variable and removed these. We corrected the flux data for density effects due to heat and water vapor transfer in the manner described in Ibrom et al. (2007). We used a footprint analysis (Kljun et al., 2015; Kormann and Meixner, 2001; Leclerc and Foken, 2014; Leclerc and Thurtell, 1990) described in sub-Section 2.4.1 to remove data where the tower footprint fell outside the fetch of the studied Spartina area. We also detected and removed spikes in the 30minute flux data using the outlier detection method Papale et al. (2006).

Some data was lost due to instrumental failure, maintenance and/or calibration. During these times, one system was usually operating and used to collect data. However, there were times where both systems were inoperative, resulting in gaps in the data. Overall, 60.1% and 42.8% of the half-hourly data was retained for further analysis in 2014 and 2015, respectively.

Gaps in climate and flux measurements in the data stream due to either unfavorable micro-meteorological conditions (i.e. low turbulence) or instrument failure needed to be filled in order to estimate seasonal and annual fluxes. We filled gaps in the time series of the flux and meteorological data using the marginal distribution sampling (MDS) gap filling algorithm (Reichstein et al., 2005) in ReddyProc* (Wutzler et al., 2018). This method combines the look-up table (LUT) algorithm described in Falge et al. (2001) with the mean diurnal variation (MDV) technique.

2.4.1. Wind direction and footprint screening

With two eddy-covariance systems on the tower, periods with wind direction from the back of one sonic anemometer were screened out due to flow distortions arising from the tower structure and filled with the data from the other eddy-covariance system on the opposite side. The system to the north covered a mean wind angle from 270 to 360 degrees and 0 to 90 degrees while the remaining wind direction was covered by the system facing south.

We used Google Earth software to determine the fetch of the area covered with *S. alterniflora* at 11.25° intervals (Figure A.2). The wind direction was used to specify the direction of the footprint with its underlying characteristic surface properties. This procedure was essential as the study area was surrounded by different types of landscape with the Duplin river approximately 300 m to the west and tidal forest approximately 1000m to the east, and we wished to include only data representing salt marsh habitats.

We applied the footprint model of Kormann and Meixner (2001) to the average 30-min of flux data to ensure that the collected data represented primarily *S. alterniflora* marsh. Contributing source signatures contained within the footprint were calculated using the equation:

$$f_x = \frac{1}{\Gamma(\mu)} \frac{\xi^{\mu}}{x^{1+\mu}} e^{-\frac{\xi}{x}} \tag{1}$$

where f_x is the fraction of flux originating from the defined study area (example 10%, 30%, 90%), x is the distance from the location of the flux system measured in the wind direction, $\xi = \xi$ (z) is a flux length scale that depends on the height above the ground z, μ is a dimensionless number and $\Gamma(\mu)$ is the gamma function. Based on the prevailing wind direction, the footprint model was applied to the google map of the flux site to screen out measurements where the source was outside the region of interest. That was done using a footprint filter with a threshold of 70% cumulative source contribution (hereafter referred to as CSC) (Ammann et al., 2007; Pahari et al., 2018).

2.5. Effect of daytime tidal inundation on CO2 fluxes

To determine the effect of daytime tidal inundation on CO_2 fluxes, we removed all night-time data (defined as net radiation (Rn) lower than 20 w m $^{-2}$). We then examined (i) the effect of daytime spring and neap tides on CO_2 fluxes, and (ii) the effect of daytime variable flooding depths on CO_2 fluxes.

2.5.1. Spring and neap tide

We defined spring tides as days with higher tides than the average value of the next 14 days; otherwise, they were regarded as neap tides (Fig. A.3). This characterization was cross checked against the moon phase and the tide table from Old Tea Kettle Creek tide station (NOAA, 2019). For each month, we examined NEE data for a period of 3-5 consecutive days (Li et al., 2014) representing spring and neap tide conditions. The number of days observed was limited and differed among months because we also faced the constraint of observing tide cycles that fell completely during daylight hours. Examples of field conditions during selected neap and spring tide days are shown in Fig. A.4.

2.5.2. Variable flooding depths

To determine the impact of variable flooding depths on CO_2 fluxes, we defined a parameter termed as the ratio of tide height h_{tide} to the plant height h_{plant} (Fig. 2). When h_{tide}/h_{plant} equals 1, the plants are completely submerged, and when h_{tide}/h_{plant} equals 0, the plants are completely exposed to the atmosphere. The NEE data was binned into four h_{tide}/h_{plant} intervals of 0.25.

We used a non-linear regression analysis using the Landsberg model

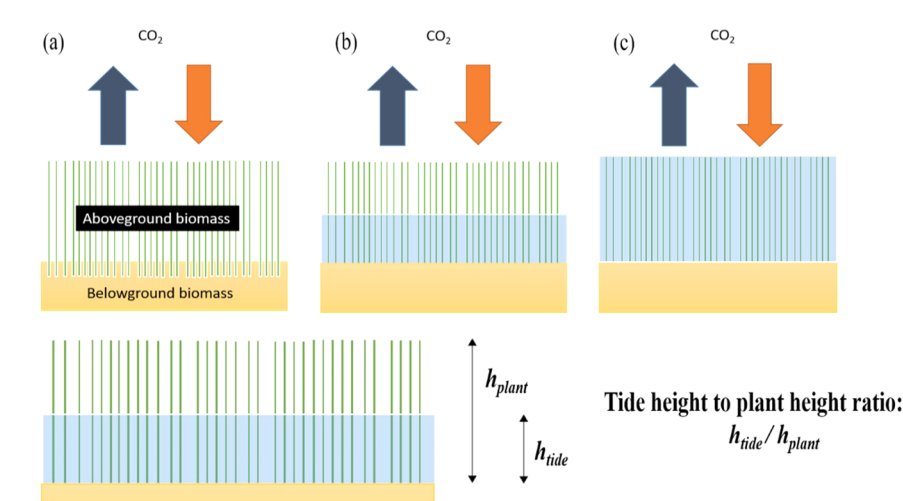


Fig. 2. Top: Different tide levels in the salt marsh affect the amount of vegetation exposed to the air; (a) Vegetation is completely exposed to the air during low spring tides and neap tides (b) Vegetation is partially submerged as the water level rises (c) Vegetation is completely submerged during high spring tides. Bottom: The tide height to plant height ratio is an index of the amount of vegetation exposed to the atmosphere. h_{tide} is the tide height and h_{plant} is monthly mean plant height.

(Chen et al., 2002) to reflect the effect of PAR on daytime CO_2 fluxes. This model was applied to the binned data of different h_{tide}/h_{plant} and non-flooded conditions. These fits were used to determine at what h_{tide}/h_{plant} the reduction of CO_2 flux occurred using the fit from non-flooded conditions as a reference. The Landsberg model is as follows:

$$NEE = P_{\text{max}} \times \left(1 - e^{(-\alpha \times (PAR - I_{comp}))}\right)$$
 (2)

where P_{max} is the maximum rate of photosynthesis (µmol m⁻² s⁻¹), α is apparent quantum yield, PAR is the photosynthetically active radiation (µmol m⁻² s⁻¹) and I_{comp} is the light compensation point. High P_{max} values and low I_{comp} values are good indicators of high carbon assimilation capacity of plants (Li et al., 2014).

We quantified the reduction of CO_2 flux as the difference between measured CO_2 flux during flooded conditions and the CO_2 flux calculated using Eq. (2) during non-flooded conditions. These differences represent the amount of CO_2 flux reduced by tide for each tide events. The calculations used the following equations:

$$F_{tide} = F_{mea} - F_{mod} \tag{3}$$

$$F_{tot} = \sum (F_{mea} - F_{mod}) \tag{4}$$

where F_{tide} is the amount of CO₂ in percentage reduced by tide for each tide events, F_{mea} is the CO₂ flux measured during flooded conditions, F_{mod} is the CO₂ flux calculated using Eq. (2) for non-flooded conditions at the same time, and F_{tot} is the total amount of CO₂ reduced by tide events. Monthly CO₂ reductions were estimated for all of 2014 and for January – September of 2015. Given that the months of October and November 2015 experienced an extreme event (prolonged flooding due to a storm) that hampered photosynthesis activity (Nahrawi, 2019), these months were omitted from the present study.

3. Results and discussion

3.1. Diurnal variations of CO2 fluxes and its relation to tide

In Georgia, the salt marsh ecosystem fixes atmospheric carbon for up to about twelve hours during the summer solstice and up to nine hours near the winter solstice (Nahrawi, 2019). Overall, carbon exchange between the salt marsh and the atmosphere reached a maximum between late morning and noon when the PAR level and air temperature were high (Nahrawi, 2019).

The effect of the tides on NEE depended on the month of the year (Fig. 3). The daytime averages of NEE were higher during neap tide periods than during spring tide periods in the months of the spring season for both years (Table 1). Flux partitioning results show that gross

primary productivity (GPP) in these months was significant higher during neap tides than during spring tides, while ecosystem respiration did not show a significant difference between neap and spring tides. This indicates suppressed photosynthetic activity during spring tides. The greatest differences in net ecosystem exchange between the neap and spring tides were observed early in the growing season (February and March). During these months, the daytime ${\rm CO}_2$ uptake during neap tides reached -7.98 μ mol m⁻² s⁻¹ and -3.99 μ mol m⁻² s⁻¹ in 2014 and 2015 respectively, versus -4.55 μ mol m⁻² s⁻¹ and -3.77 μ mol m⁻² s⁻¹ during spring tides. A similar pattern was observed during April in 2015 and May of both years. However, in April 2014, the CO2 uptake was greater during the spring tide than the neap tide. During this month, rainfall was high during the spring tide cycle, likely reducing pore water salinity and allowing high CO2 uptake, as reported in New England salt marshes (Forbrich et al., 2018). The differences in NEE between the two tidal phases were small from June onwards for both years except for September 2015.

Guo et al. (2009) found a different pattern than ours, with daytime C uptake greater during spring tide than neap tide early in the season, and greater during neap tide than spring tide late in the season. Guo et al. (2009) report samples taken over a four-month period (January, April, July and October), making a meaningful comparison with our findings difficult. The most likely explanation for the seasonal pattern observed in our study lies in the fact that plants were relatively short early in the growing season (Figure 4) and therefore flooded more completely at high tide. During the summer, the vegetation was taller and may also have been more acclimated to environmental changes such as tidal inundation, leading to smaller differences in NEE between neap and spring tide periods. S. alterniflora has a well-developed system of aerenchyma which functions as a canal for gas exchange between the plant and the rhizosphere (Guo et al., 2009; Mendelsohn and Postek, 1982). It is possible that this system is better developed in the summer than the spring, leading to a greater tolerance of flooding later in the growing season, although we are not aware of any study that examines this possibility.

3.2. Effect of variable flooding on NEE

Our findings suggest that net ecosystem exchange is not simply a function of spring versus neap tides: rather, NEE varies continuously with both PAR and the level of flooding (Figs. 5, 6). We found that NEE increased (more negative) with greater PAR, as would be expected. As the ratio of the tide level to the plant height increased, NEE decreased (less negative). This effect of variable flooding was greatest in the spring (March-May) and fall (September), with tidal flooding having a

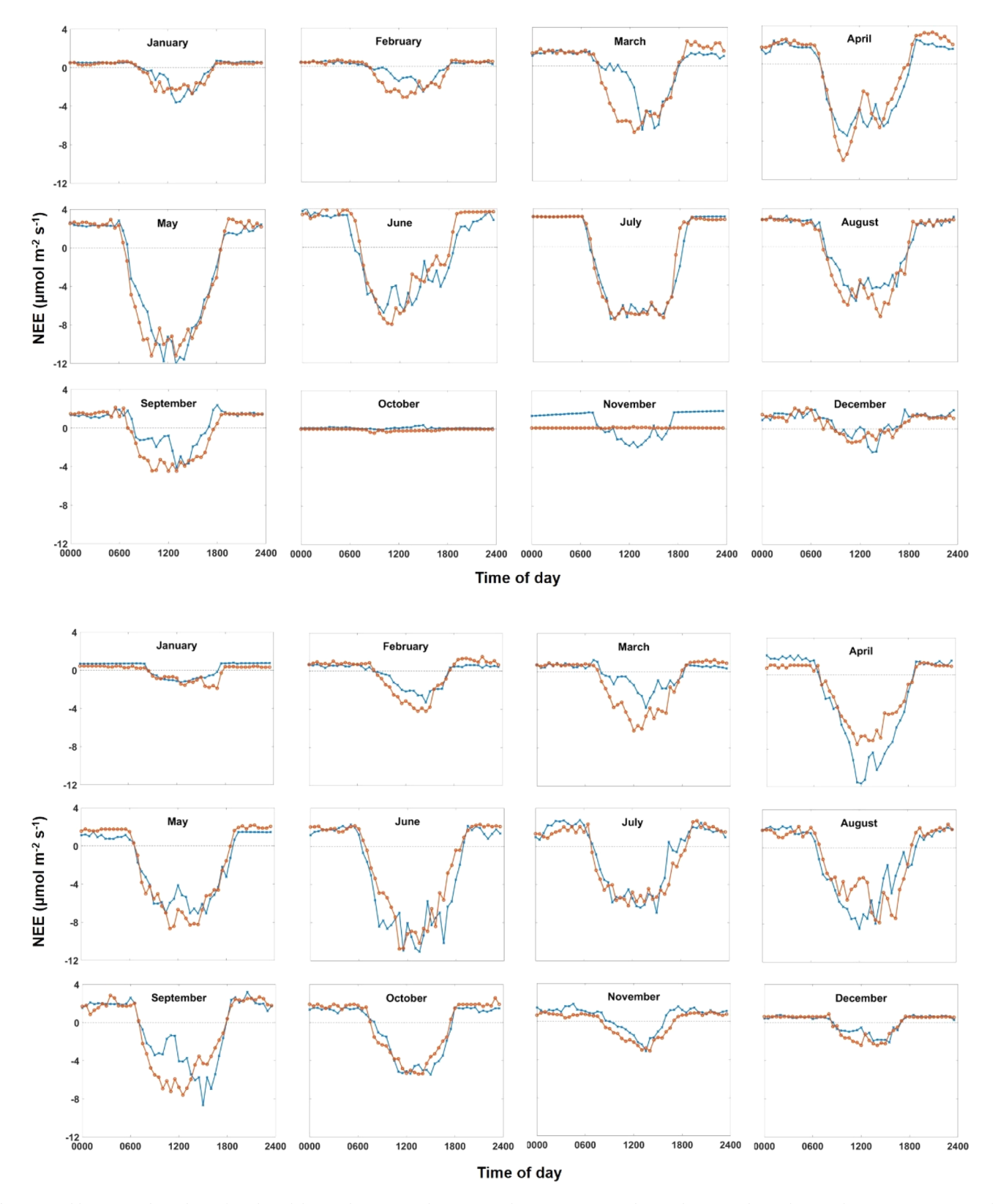


Fig. 3. Monthly average diurnal NEE for selected days within spring tides or neap tides in 2014 (top) and 2015 (bottom). Blue and orange lines represent spring tides and neap tides, respectively.

minor impact on NEE during summer and winter.

In particular, from March to May and in September for both years, NEE decreased (less negative) at a low ratio of tide height to plant height (0 < $h_{\rm tide}/h_{\rm plant} <$ 0.25). In July and June 2014, NEE started to

decrease (less negative) when the h_{tide}/h_{plant} value was greater, 0.25
 $h_{tide}/h_{plant}\!<\!0.5.$ No net ecosystem exchange reduction due to flooding was observed in June and July 2015 at any level of $h_{tide}/h_{plant}.$

A comparison of P_{max} α and I_{comp} values obtained from the

Table 1 Monthly average of net ecosystem exchange (NEE, μ mol m⁻² s⁻¹), respiration (Re, μ mol m⁻² s⁻¹), and gross primary productivity (GPP, μ mol m⁻² s⁻¹) for daytime spring and neap tides of 2014 and 2015. SE is standard error around mean. Values in bold indicate significantly higher NEE (more negative), Re and GPP (more negative) between spring and neap tides. Means with different letters are significant in different at p<0.05 using the Tukey method.

Year	Month	Day of Month	Tide	NEE (μ mol m ⁻² s ⁻¹)		Re (μ mol m ⁻² s ⁻¹)		GPP (μ mol m ⁻² s ⁻¹)	
				Mean	SE	Mean	SE	Mean	SE
2014	January	3-5	Spring	-0.76 ^a	0.06	0.72 ^a	0.04	-1.49 ^a	0.06
		22-24	Neap	-0.98 ^a	0.11	0.45 ^b	0.02	-1.42 ^a	0.11
	February	26-28	Spring	-1.41 ^a	0.18	$0.57^{\rm b}$	0.02	-1.98 ^b	0.18
		18-20	Neap	-2.04 ^a	0.27	1.27 ^a	0.04	-3.32 ^a	0.30
	March	1-3	Spring	-1.26 ^b	0.21	0.80^{a}	0.03	-2.06 ^b	0.21
		9-11	Neap	-3.34 ^a	0.29	1.29^{a}	0.04	-4.63 ^a	0.31
	April	26-28	Spring	-6.10 ^b	0.46	1.90^{a}	0.03	-7.99 ^a	0.48
		9-11	Neap	-4.06 ^a	0.30	1.16 ^a	0.03	-5.22 ^b	0.31
	May	16-18	Spring	-4.32 ^b	0.31	1.34 ^a	0.03	-5.66 ^b	0.33
		5-7	Neap	-5.25 ^a	0.34	2.38^{a}	0.05	-7.63 ^a	0.37
	June	14-16	Spring	-6.39 ^a	0.48	2.07^{a}	0.02	-8.47 ^a	0.49
		4-6	Neap	-5.41 ^a	0.48	2.14 ^a	0.04	-7.55 ^a	0.50
	July	14-16	Spring	-3.28 ^a	0.38	1.96 ^a	0.02	-5.24 ^a	0.40
		2-4	Neap	-3.50 ^a	0.31	2.05^{a}	0.03	-5.55 ^a	0.32
	August	7-9	Spring	-4.47 ^a	0.34	2.15^{a}	0.03	-6.62 ^a	0.36
	-	17-19	Neap	-3.86 ^a	0.36	1.99 ^a	0.03	-5.85 ^a	0.38
	September	10-12	Spring	-3.42 ^a	0.33	2.42 ^a	0.03	-5.84 ^a	0.34
	•	1-3	Neap	-4.30 ^a	0.41	2.44 ^a	0.03	-6.74 ^a	0.43
	October	5-7	Spring	-3.15 ^a	0.31	1.44 ^a	0.04	-4.59 ^a	0.33
		16-18	Neap	-2.98 ^a	0.25	2.15^{a}	0.06	-5.14 ^a	0.28
	November	4-6	Spring	-2.41 ^a	0.25	1.41 ^a	0.03	-3.81a	0.27
		27-29	Neap	-1.16 ^a	0.11	0.73^{a}	0.02	-1.89 ^b	0.12
	December	8-10	Spring	-0.96 ^a	0.11	0.66 ^a	0.02	-1.62 ^b	0.12
		13-15	Neap	-1.33 ^a	0.14	0.99^{a}	0.04	-2.32a	0.17
2015	January	19-21	Spring	-1.35 ^a	0.19	0.87^{a}	0.03	-2.22 ^a	0.21
	Ĭ	26-28	Neap	-1.50 ^a	0.15	0.63 ^a	0.02	-2.13 ^a	0.16
	February	18-20	Spring	-0.91 ^b	0.12	0.50^{a}	0.02	-1.42 ^b	0.11
	•	11-13	Neap	-1.87 ^a	0.15	0.71 ^a	0.04	-2.58a	0.17
	March	20-22	Spring	-2.14 ^b	0.38	1.43 ^a	0.02	-3.57 ^b	0.39
		9-11	Neap	-3.88 ^a	0.32	2.14 ^a	0.05	-6.03 ^a	0.35
	April	21-23	Spring	-4.18 ^b	0.33	2.43 ^a	0.04	-6.70 ^a	0.36
	•	8-10	Neap	-5.28 ^a	0.45	2.89 ^a	0.04	-7.07 ^a	0.47
	May	17-19	Spring	-5.99 ^b	0.53	2.62 ^a	0.03	-8.61 ^a	0.55
	·	26-28	Neap	-6.52a	0.52	2.29 ^a	0.02	-8.81 ^a	0.53
	June	15-17	Spring	-3.56 ^a	0.33	3.81 ^a	0.05	-7.38 ^a	0.35
		24-26	Neap	-3.64 ^a	0.47	4.20 ^a	0.06	-7.84 ^a	0.52
	July	28-30	Spring	-4.63 ^a	0.35	3.11 ^a	0.02	-7.73 ^a	0.36
		22-24	Neap	-4.72 ^a	0.39	3.43 ^a	0.06	-8.15 ^a	0.42
	August	27-29	Spring	-2.64 ^a	0.36	2.97 ^a	0.03	-5.61 ^b	0.38
	. 0	20-22	Neap	-3.45 ^a	0.34	3.65 ^a	0.04	-7.10 ^a	0.38
	September	28-30	Spring	-1.14 ^a	0.26	1.63 ^a	0.02	-2.76 ^b	0.26
	r	20-22	Neap	-2.75 ^b	0.21	1.99 ^a	0.04	-4.74 ^a	0.22

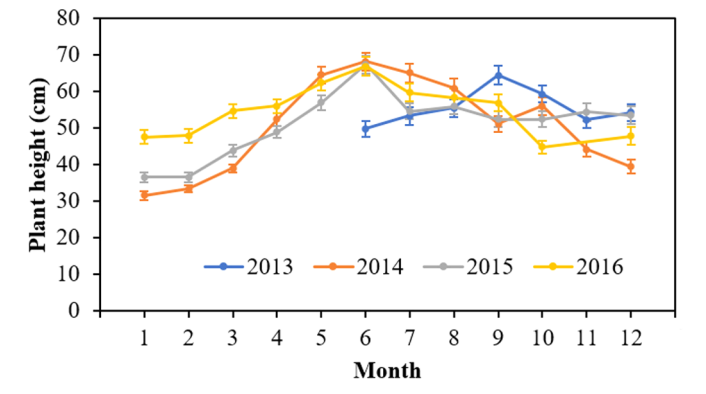


Fig. 4. The averages and their standard errors of *Spartina alterniflora* plant height from June to December of 2013 and January to December of 2014, 2015, and 2016.

regression analyses further confirms this pattern (Tables A.1, A.2). In most months, P_{max} had negative values and its magnitude decreased from non-flooded conditions to higher $h_{\rm tide}/h_{\rm plant}$ levels, while $I_{\rm comp}$ values increased. High P_{max} values and low I_{comp} valuesare good

indicators of high carbon assimilation capacity of plants (Li et al., 2014). The significantly low P_{max} and high values of I_{comp} obtained from the regression analysis of the NEE-PAR relationship indicate that the carbon assimilation capacity of this salt mash was reduced at higher levels of $h_{\rm tide}/h_{\rm plant}$.

In this study, we determined that tidal flooding reduces CO_2 exchange. In particular, our results supported the hypotheses that daytime CO_2 exchange in an intertidal salt marsh ecosystem would be related to the amount of vegetation exposed to the atmosphere, to light intensity, and to the seasonal growth cycle of the plant. Tidal water at the study site is quite turbid, so light penetration through the water is quite low (Tweedley et al., 2016). As a result, submergence of leaves reduced light interception in addition to reducing CO_2 transport through stomata and the availability of oxygen to roots and rhizomes. Some of the measured NEE was also likely contributed by benthic microalgae (Joye et al., 2003), and these would also have experienced reduced light availability during tidal flooding.

Although we found that NEE was reduced (less negative) during tidal flooding, studies of plant productivity at the annual scale often find increased production during years with relatively high sea levels or in areas with moderately high tidal flooding (Li et al., 2018; Morris et al., 2013; Wieski and Pennings, 2013). Explanations for the latter result typically emphasize dilution of salts or increased fluxes of

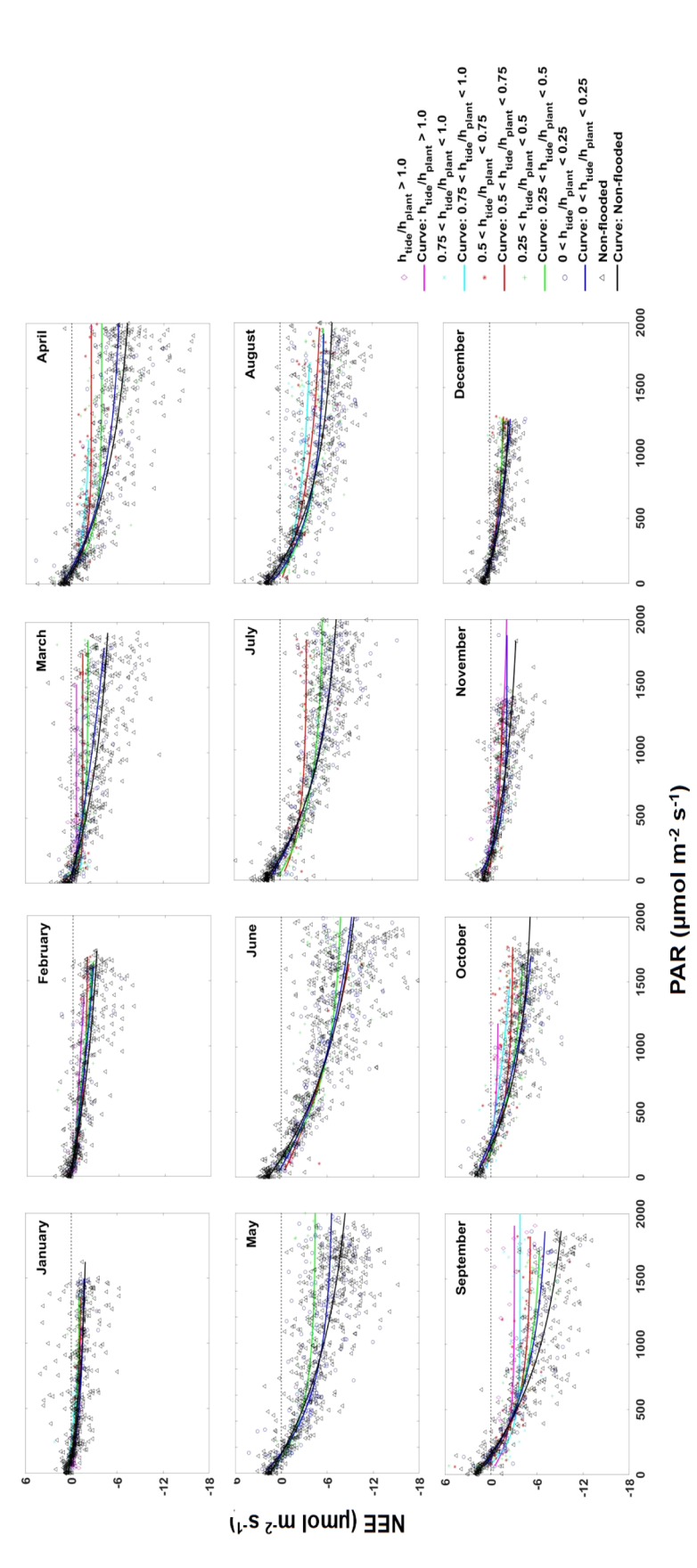
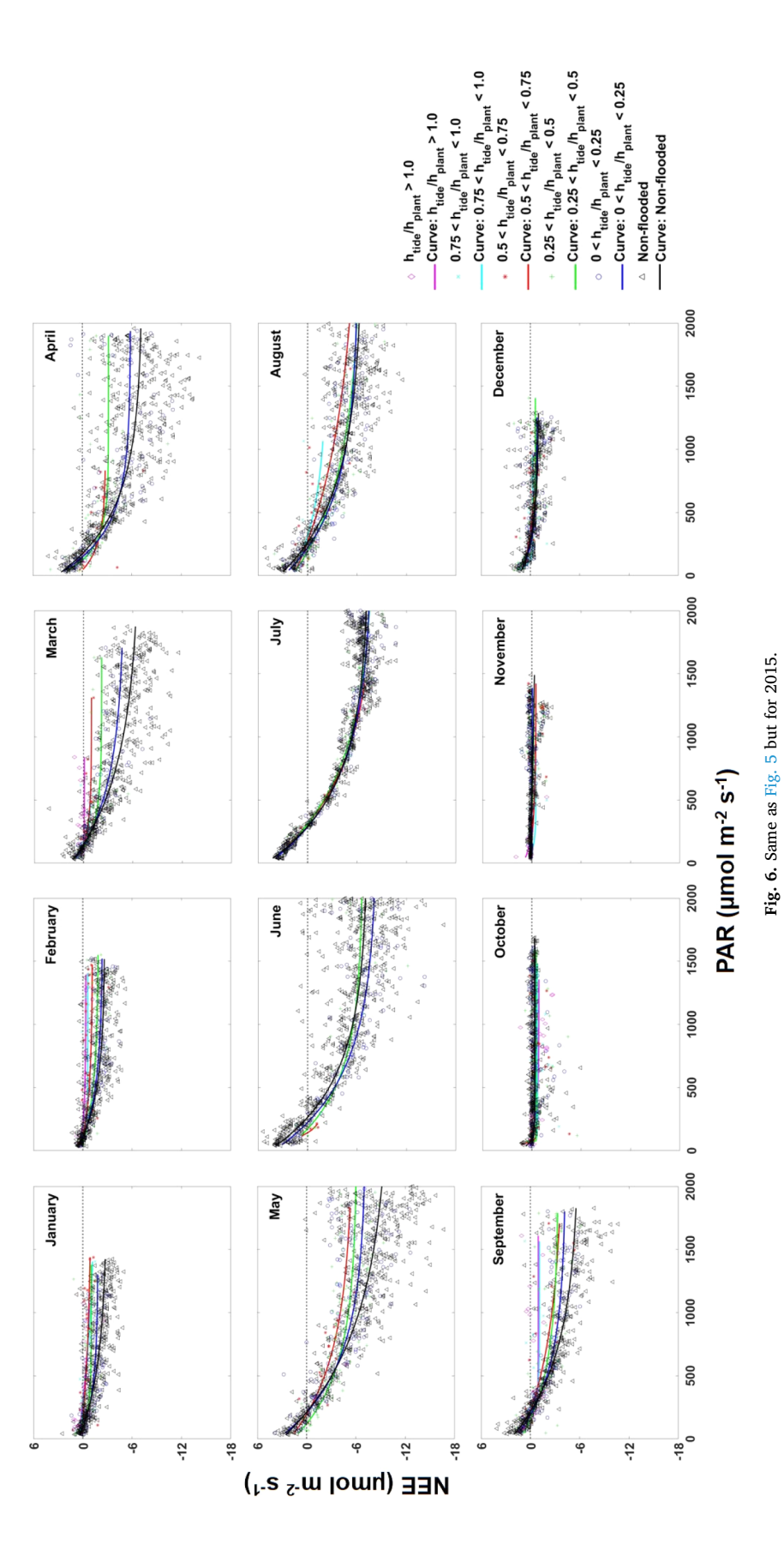


Fig. 5. Monthly daytime NEE versus PAR partitioned by htide/hplant for 2014. Curves fit from nonlinear regression analysis of daytime NEE versus PAR based on equation (2) (the Landsberg model) are included.



8

Table 2 Monthly reduction in NEE as a function of the tide height to plant height ratio. F_{mod} is CO_2 flux calculated using equation (2). F_{mea} is CO_2 flux measured during flooded conditions. F_{tide} is the amount of CO_2 flux reduced by high tides for each tide event. $\%F_{tide}$ is percent of F_{tide} change from F_{mod} (non-flooded condition). SE is the standard error of the mean. Values in bold indicate a higher reduction of CO_2 flux.

Year	Month	F_{mea}	SE	F_{mod}	SE	F_{tide}	% F _{tide}
2014	February	-72.78	0.10	-97.28	0.12	24.50	25.19
	March	-161.63	0.09	-259.71	0.14	98.08	37.77
	April	-272.01	0.17	-420.01	0.21	148.00	35.24
	May	-133.15	0.27	-190.56	0.42	57.41	30.13
	June	-395.60	0.39	-423.88	0.41	28.28	6.67
	July	-265.07	0.21	-317.68	0.30	52.61	16.56
	August	-602.06	0.17	-707.78	0.18	105.72	14.94
	September	-617.18	0.16	-861.56	0.23	244.39	28.37
	October	-512.83	0.13	-641.13	0.13	128.30	25.02
2015	Jan	-37.13	0.08	-119.88	0.11	82.75	19.03
	February	-69.04	0.10	-141.40	0.11	72.37	51.18
	March	-48.95	0.12	-134.21	0.19	85.26	63.53
	April	-135.59	0.27	-173.46	0.36	37.86	21.83
	May	-344.75	0.27	-440.23	0.36	95.48	21.69
	June	-108.62	0.58	-125.98	0.63	17.36	15.98
	July	-189.07	0.44	-191.52	0.42	2.46	1.28
	August	-215.30	0.28	-234.87	0.29	19.57	8.33
	September	-161.38	0.16	-275.21	0.21	113.83	41.36

oxygen or nutrients during periods of increased flooding. The resolution of this contrast between short-term eddy-covariance results and long-term harvest results may be due to tidal flooding improving average abiotic conditions despite reducing NEE during the relatively short period during which the marsh is flooded most deeply.

3.3. Tide-induced reduction of daytime CO₂ exchange

The monthly reduction of daytime CO_2 flux due to high tides in 2014 was greatest in March (38%), followed by April (35%) and May (30%), while a lesser reduction was observed during the summer months (June 7%, July 17% and August 15%) (Table 2). A similar pattern occurred in 2015.

In a preliminary study, we reported that when the marsh was flooded 0.2 m deep, CO₂ exchange started to decrease (Nahrawi, 2019). This observation was from summer 2014 when a high tide occurred during midday with high PAR and temperature, i.e., conditions representing the greatest potential for CO2 reduction. The observed flooding depth required to reduce NEE (less negative) was similar to values reported by Kathilankal et al. (2008) and higher than the values of 0.17 m and 0.05 m reported by Moffett et al. (2010) and Forbrich and Giblin (2015) respectively. Kathilankal et al. (2008) studied a similar ecosystem to the S. alterniflora marsh studied here, and thus a similar pattern in the reduction of CO2 flux during flooding can be expected. These previous studies reported only one water level threshold when NEE started to decrease (less negative). However, in the present study we found that the effect of flooding was continuous rather than stepwise. We also found that the effect of flooding on NEE varied seasonally. The highest CO2 flux reduction was observed during the early and peak parts of the growing season (February, March, April and May), with a lower effect during the summer in both years. Overall, our

findings suggest that daytime CO_2 flux was reduced (less negative) 20-60% by flooding during the peak growing season.

4. Conclusions

Net ecosystem exchange in salt marshes varies on multiple time scales. Several variables such as photosynthetically active radiation, temperature and tide height all interact with plant phenology over the growing season to impact NEE on daily, monthly and annual scales. In this manuscript, we emphasised the roles of both tide height and seasonality, building on previous studies that have examined the roles of PAR and temperature (Nahrawi, 2019).

One key finding was that increasing tidal flooding reduces NEE (less negative); we also determined that this effect differs with the season. Net ecosystem exchange was up to 63% greater during neap tides than spring high tides, with the largest difference occurring early in the growing season. Tidal flooding varies continuously, affecting the degree to which plants are inundated versus emergent. The effect of flooding was also continuous rather than stepwise. The total monthly reduction in NEE due to tidal flooding was 7-38% and 1-64% for 2014 and 2015 respectively. The higher $\rm CO_2$ flux reductions were observed during early to peak growing season (February, March, April and May) and lower reductions were observed during the summer of both years. Overall, our findings suggest that the daytime $\rm CO_2$ flux was reduced (less negative) 20-60% during the peak growing season due to tidal flooding.

Our results suggest that marshes will be most vulnerable to high sea levels in the spring season. A more sophisticated understanding of the temporal dynamics of sea level variation may thus allow a better understanding of temporal variation in plant productivity, and ultimately of the prospects for marsh survival in areas with rapid sea level rise. Further work should include a more comprehensive analysis of the total carbon balance over a full daily cycle and should also address lateral transport of carbon by the tides. In addition, there is a striking disconnect between the results reported here (tidal flooding reduces NEE (less negative)) and the results of annual survey and harvest studies (moderate tidal flooding improves plant productivity): the different conclusions may be due to the differing temporal scales of the two types of studies, but these contrasting results deserve more attention.

Declaration of Competing Interest

The authors declare that they have no conflict of interest.

Acknowledgments

This study is based upon work supported by the National Science Foundation through the Georgia Coastal Ecosystems Long-Term Ecological Research program under Grant No. OCE12-37140. We thank the UGA Marine Institute (contribution no. 1061) for providing us with accommodation and laboratory facilities during our fieldwork. Thanks to our PI Merryl Alber and to Daniela Di Iorio, who supported us in many ways and provided us with great research facilities. Finally, we thank Wade Sheldon, Jacob Shalack, Timothy Montgomery and Mohamad Widya Iskandar for help with data management and field work.

Appendices

Tables A1 and A2, Figs. A1-A4.

Table A.1 Monthly parameters and values using the Landsberg model fitted to the daytime net ecosystem change of CO_2 (NEE) based on photosynthetic active radiation (PAR) for different tide height to plant height ratio (h_{tide}/h_{plant}) in 2014. P_{max} is the maximum rate of photosynthesis, α is apparent quantum yield and I_{comp} is the light compensation point. na – no data available.

Month	h_{tide}/h_{plant}	P_{max}	α	I_{comp}	\mathbb{R}^2	n
Feb	>1	na	na	na	0.30	22
	0.75-1	na	na	na	0.23	7
	0.5-0.75	-2.99	0.0019	139.17	0.50	11
	0.25-0.5	-4.72	0.0001	128.20	0.61	33
	0-0.25	-6.44	0.0004	104.01	0.44	54
	no flood	-4.31	0.0008	100.71	0.52	455
Mar	>1	na	na	na	0.06	28
	0.75-1	-1.41	0.0309	69.76	0.53	16
	0.5-0.75	-1.51	0.0130	67.13	0.52	21
	0.25-0.5	na	na	na	0.24	50
	0-0.25	-5.81	0.0003	66.25	0.59	77
	no flood	-9.67	0.0009	66.07	0.48	512
Apr	0.75-1	na	na	na	0.36	13
	0.5-0.75	-2.54	0.0048	135.56	0.45	39
	0.25-0.5	-3.92	0.0038	126.38	0.39	53
	0-0.25	-6.56	0.0014	101.09	0.60	84
	no flood	-8.42	0.0010	94.46	0.68	566
May	0.25-0.5	-4.48	0.0025	156.08	0.71	41
	0-0.25	-6.77	0.0019	148.95	0.57	154
	no flood	-10.11	0.0009	120.02	0.72	629
Jun	0.5-0.75	na	na	na	0.29	8
	0.25-0.5	-8.09	0.0017	147.78	0.57	58
	0-0.25	-11.53	0.0008	132.55	0.67	136
	no flood	-11.56	0.0009	76.52	0.68	617
July	0.5-0.75	na	na	na	0.20	14
	0.25-0.5	-5.69	0.0018	173.69	0.73	61
	0-0.25	-8.41	0.0011	148.22	0.71	127
	no flood	-8.21	0.0012	54.26	0.78	642
Aug	0.75-1	na	na	na	0.31	23
	0.5-0.75	-5.72	0.0012	143.75	0.53	37
	0.25-0.5	-5.76	0.0021	144.82	0.55	82
	0-0.25	-5.85	0.0020	87.38	0.52	137
	no flood	-7.27	0.0015	62.67	0.70	517
Sep	>1	na	na	na	0.13	31
	0.75-1	-3.80	0.0051	145.53	0.54	42
	0.5-0.75	-5.19	0.0026	125.42	0.70	62
	0.25-0.5	-6.77	0.0017	138.44	0.77	67
	0-0.25	-7.62	0.0015	125.50	0.79	84
	no flood	-10.82	0.0011	160.12	0.81	409
Oct	>1	-0.95	0.0036	283.81	0.64	10
	0.75-1	-5.54	0.0005	256.31	0.46	17
	0.5-0.75	na	na	na	0.34	61
	0.25-0.5	-4.71	0.0014	205.14	0.54	66
	0-0.25	-7.08	0.0009	287.18	0.61	88
	no flood	-5.59	0.0014	237.06	0.74	432
Nov	>1	na	na	na	0.26	31
	0.75-1	na	na	na	0.28	27
	0.5-0.75	-1.56	0.0023	157.34	0.47	33
	0.25-0.5	-2.11	0.0032	169.34	0.49	52
	0-0.25	-2.10	0.0035	210.18	0.48	54
	no flood	-3.94	0.0011	220.75	0.53	403

Table A.2 Monthly parameters and values using the Landsberg model fitted to the daytime net ecosystem change of CO_2 (NEE) based on photosynthetic active radiation (PAR) for different tide height to plant height ratio (h_{tide}/h_{plant}) in 2015. P_{max} is the maximum rate of photosynthesis, α is apparent quantum yield and I_{comp} is the light compensation point. na – no data available.

Month	h_{tide}/h_{plant}	P_{max}	α	I_{comp}	\mathbb{R}^2	n
Jan	>1	-1.26	0.0013	279.24	0.37	21
	0.75-1	-1.70	0.0010	225.81	0.69	13
	0.5-0.75	-1.11	0.0012	153.75	0.28	16
	0.25-0.5	-1.03	0.0075	122.98	0.30	27
	0-0.25	-1.82	0.0034	92.67	0.41	70
	no flood	-3.00	0.0018	87.64	0.56	429
Feb	>1	-0.37	0.0042	219.28	0.48	9
	0.75-1	-0.59	0.0109	111.84	0.29	14
	0.5-0.75	-1.18	0.0026	107.30	0.32	28
	0.25-0.5	-1.91	0.0024	62.39	0.39	30
	0-0.25	-2.42	0.0025	90.77	0.51	57
	no flood	-2.69	0.0026	53.25	0.55	419
Mar	>1	na	na	na	0.03	19
	0.75-1	na	na	na	0.25	9
	0.5-0.75	-0.97	0.0052	151.12	0.62	11
	0.25-0.5	-2.21	0.0046	139.29	0.51	30
	0-0.25	-4.99	0.0018	148.22	0.67	52
	no flood	-6.97	0.0014	125.36	0.67	556
Apr	0.5-0.75	na	na	na	0.26	13
	0.25-0.5	-3.19	0.0053	173.72	0.41	42
	0-0.25	-5.86	0.0030	147.95	0.54	78
	no flood	-7.28	0.0021	122.50	0.61	565
May	>1	na	na	na	0.30	2
	0.75-1	-1.46	0.0271	212.06	0.91	2
	0.5-0.75	-5.70	0.0016	194.67	0.72	13
	0.25-0.5	-6.14	0.0020	119.34	0.68	70
	0-0.25	-7.26	0.0019	128.97	0.58	122
	no flood	-10.32	0.0012	76.58	0.69	597
Jun	0.5-0.75	-2.08	0.0121	222.93	0.86	1
	0.25-0.5	-6.72	0.0021	263.69	0.63	25
	0-0.25	-8.47	0.0018	171.87	0.66	87
	no flood	-7.32	0.0019	141.38	0.69	658
Jul	0.75-1	-4.70	0.0024	297.37	0.99	4
	0.5-0.75	-8.61	0.0015	309.96	0.99	14
	0.25-0.5	-8.24	0.0014	310.25	0.95	38
	0-0.25	-7.94	0.0016	284.90	0.92	90
	no flood	-7.49	0.0018	290.13	0.93	633
Aug	0.75-1	na	na	na	0.35	3
	0.5-0.75	-6.57	0.0009	271.10	0.67	26
	0.25-0.5	-6.62	0.0013	264.54	0.68	50
	0-0.25	-6.19	0.0018	189.97	0.79	98
	no flood	-6.71	0.0016	219.91	0.77	573
Sep	>1	na	na	na	0.22	23
	0.75-1	na	na	na	0.26	11
	0.5-0.75	-4.16	0.0013	221.42	0.57	20
	0.25-0.5	-3.46	0.0020	152.16	0.49	56
	0-0.25	-4.33	0.0020	189.09	0.75	81
	no flood	-6.02	0.0016	145.77	0.75	478



Fig. A.1. Eddy-covariance system installed in the Sapelo Island salt marsh ecosystem.

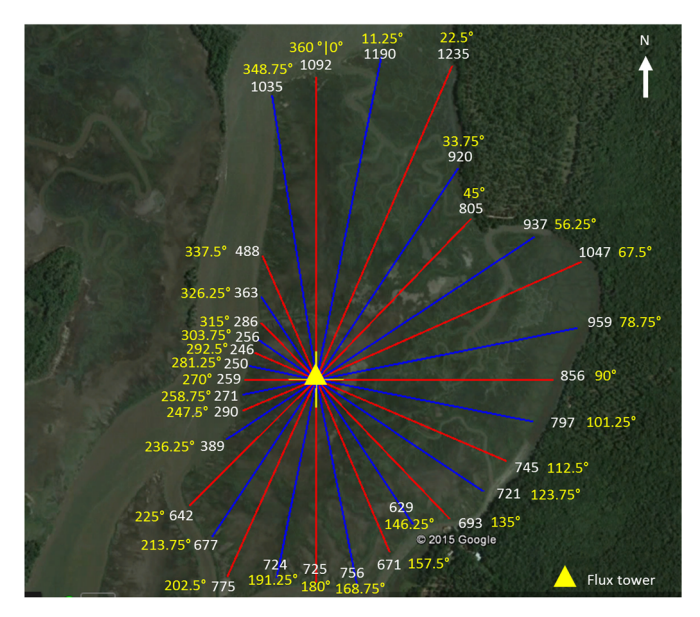


Fig. A.2. Fetch of the study area. The numbers in white are the approximate distance from the flux tower to the boundary of the study area in meters. The numbers in yellow are the angle for each distance.

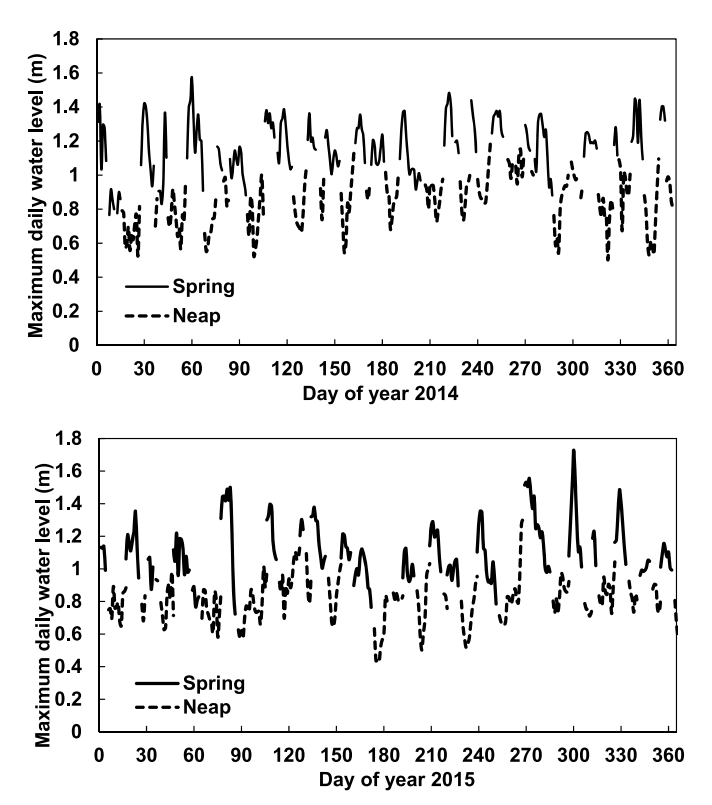


Fig. A.3. The differentiation of spring and neap tide periods at the study site in 2014 (top) and 2015 (bottom) based on the maximum daily water levels.



Fig. A.4. Views of the salt marsh from the flux tower during daytime high spring and neap tide periods. Photos were taken at (a) 1200 EST on May 17, 2014 during a spring tide, (b) 1000 EST on October 25, 2014 during a spring tide, (c) 1000 EST on May 4, 2014 during a neap tide, and (d) 1000 EST on October 16, 2014 during a neap tide.

References

Ammann, C., Flechard, C.R., Leifeld, J., Neftel, A., Fuhrer, J., 2007. The carbon budget of newly established temperate grassland depends on management intensity. Agric. Ecosyst. Environ. 121, 5–20. https://doi.org/10.1016/J.AGEE.2006.12.002.

Bortolus, A., Adam, P., Adams, J.B., Ainouche, M.L., Ayres, D., Bertness, M.D., Bouma, T.J., Bruno, J.F., Caçador, I., Carlton, J.T., Castillo, J.M., Costa, C.S.B., Davy, A.J., Deegan, L., Duarte, B., Figueroa, E., Gerwein, J., Gray, A.J., Grosholz, E.D., Hacker, S.D., Hughes, A.R., Mateos-Naranjo, E., Mendelssohn, I.A., Morris, J.T., Muñoz-Rodríguez, A.F., Nieva, F.J.J., Levin, L.A., Li, B., Liu, W., Pennings, S.C., Pickart, A., Redondo-Gómez, S., Richardson, D.M., Salmon, A., Schwindt, E., Silliman, B.R., Sotka, E.E., Stace, C., Sytsma, M., Temmerman, S., Turner, R.E., Valiela, I., Weinstein, M.P., Weis, J.S., 2019. Supporting Spartina: Interdisciplinary perspective shows Spartina as a distinct solid genus. Ecology 100. https://doi.org/10.1002/ecv.2863.

Cai, W.-J., 2011. Estuarine and coastal ocean carbon paradox: CO₂ sinks or sites of terrestrial carbon incineration? Ann. Rev. Mar. Sci. 3, 123–145. https://doi.org/10. 1146/annurev-marine-120709-142723.

Chalmers, A.G., 1997. The ecology of the Sapelo Island National Estuarine Research Reserve. National Oceanic and Athmospheric Administration.

Chmura, G.L., Anisfeld, S.C., Cahoon, D.R., Lynch, J.C., 2003. Global carbon sequestration in tidal, saline wetland soils. Global Biogeochem. Cycles 17, 1111. https://doi.org/10.1029/2002GB001917.

Duarte, C.M., Middelburg, J.J., Caraco, N., 2005. Major role of marine vegetation on the oceanic carbon cycle. Biogeosciences 2, 1–8. https://doi.org/10.5194/bg-2-1-2005.

Falge, E., Baldocchi, D., Olson, R., Anthoni, P., Aubinet, M., Bernhofer, C., Burba, G., Ceulemans, R., Clement, R., Dolman, H., Granier, A., Gross, P., Grünwald, T., Hollinger, D., Jensen, N.-O., Katul, G., Keronen, P., Kowalski, A., Ta Lai, C., Law, B.E., Meyers, T., Moncrieff, J., Moors, Eddy, William Munger, J., Pilegaard, K., Rannik, Ü., Rebmann, C., Suyker, A., Tenhunen, J., Tu, K., Verma, S., Vesala, T., Wilson, K., Wofsy, S., Schulze, E., Moors, Ej, Elbers, J.A., Ceulemans AmeriFlux, R., Munger, B., Law, B., Oren, R., 2001. Gap filling strategies for defensible annual sums of net ecosystem exchange. Agri. Forest Meteorol. 107 (1), 43–69.

Forbrich, I., Giblin, A.E., 2015. Marsh-atmosphere CO₂ exchange in a New England salt marsh. J. Geophys. Res. Biogeosciences 120, 1825–1838. https://doi.org/10.1002/ 2015.IG003044

Forbrich, I., Giblin, A.E., Hopkinson, C.S., 2018. Constraining marsh carbon budgets using long-term C burial and contemporary atmospheric CO_2 fluxes. J. Geophys. Res. Biogeosciences 123, 867–878. https://doi.org/10.1002/2017JG004336.

Guo, H., Noormets, A., Zhao, B., Chen, J., Sun, G., Gu, Y., Li, B., Chen, J., 2009. Tidal effects on net ecosystem exchange of carbon in an estuarine wetland. Agric. For. Meteorol. 149, 1820–1828. https://doi.org/10.1016/j.agrformet.2009.06.010.

Ibrom, A., Dellwik, E., Larse, S.E., Pilegaard, K., 2007. On the use of the Webb Pearman-Leuning theory for closed-path eddy correlation measurements. Tellus Series B-Chemical and Physical Meteorology 59, 937–946.

Edited byJoye, S.B., Weston, N.B., Joye, S., Porubsky, W., Weston, N., Lee, R., 2003.

Benthic microalgal production and nutrient dynamics in intertidal sediments. In: Rullkötter, J. (Ed.), Biogeochemistry of tidal flats, pp. 67–70 Edited by.

Kathilankal, J.C., Mozdzer, T.J., Fuentes, J.D., D'Odorico, P., McGlathery, K.J., Zieman, J.C., 2008. Tidal influences on carbon assimilation by a salt marsh. Environ. Res. Lett. 3, 044010. https://doi.org/10.1088/1748-9326/3/4/044010.

Kljun, N., Calanca, P., Rotach, M.W., Schmid, H.P., 2015. A simple two-dimensional parameterisation for Flux Footprint Prediction (FFP). Geosci. Model Dev. 8, 3695–3713. https://doi.org/10.5194/gmd-8-3695-2015.

Kormann, R., Meixner, F.X., 2001. An analytical footprint model for non-neutral stratification. Boundary-Layer Meteorol 99, 207–224. https://doi.org/10.1023/A:1018991015119

Leclerc, M.Y., Foken, T., 2014. Footprints in micrometeorology and ecology. Springer, Berlin Heidelberg, Berlin, Heidelberg. https://doi.org/10.1007/978-3-642-54545-0.

Leclerc, M.Y., Thurtell, G.W., 1990. Footprint prediction of scalar fluxes using a Markovian analysis. Boundary-Layer Meteorol 52, 247–258. https://doi.org/10. 1007/BF00122089.

Li, Q., Lu, W., Chen, H., Luo, Y., Lin, G., 2014. Differential responses of net ecosystem exchange of carbon dioxide to light and temperature between spring and neap tides in subtropical mangrove forests. Sci. World J. 2014, 943697. https://doi.org/10. 1155/2014/943697.

Li, S., Hopkinson, C.S., Schubauer-Berigan, J.P., Pennings, S.C., 2018. Climate drivers of Zizaniopsis miliacea biomass in a Georgia, U.S.A. tidal fresh marsh. Limnol. Oceanogr. 63, 2266–2276. https://doi.org/10.1002/lno.10937.

Mendelssohn, I.A., Postek, M.T., 1982. Elemental Analysis of Deposits on the Roots of Spartina alterniflora Loisel. Am. J. Bot. 69, 904. https://doi.org/10.2307/2442887.

Moffett, K.B., Wolf, A., Berry, J.a., Gorelick, S.M., 2010. Salt marsh-atmosphere exchange of energy, water vapor, and carbon dioxide: Effects of tidal flooding and biophysical controls. Water Resour. Res. 46, 1–18. https://doi.org/10.1029/2009WR009041.

Morris, J.T., Sundberg, K., Hopkinson, C.S., 2013. Salt marsh primary production and its response to relative sea level and nutrients in estuaries at Plum Island, Massachusets, and North Inlet, South Carolina, USA. Oceanography 26, 78–84. https://doi.org/10. 5670/oceanog.2013.48.

Nahrawi, H., 2010. Exchange of carbon dioxide between a southeastern salt marsh and the atmosphere. PhD thesis. The University of Georgia.

NOAA, 2019. Tide predictions annual tide tables - NOAA tides & currents [www document]. URL:https://www.tidesandcurrents.noaa.gov/noaatideannual.html?id = 8675365 (accessed 1.12.19).

NOAA, 2016. System-wide monitoring program [www document]. NOAA Natl. Estuar. Res. Syst. Cent. Data Manag. Off.

O'Connell, J.L., Alber, M., Pennings, S.C., 2019. Microspatial differences in soil temperature cause phenology change on par with long-term climate warming in salt marshes. Ecosystems. https://doi.org/10.1007/s10021-019-00418-1.

Pahari, R., Leclerc, M.Y., Zhang, G., Nahrawi, H., Raymer, P., 2018. Carbon dynamics of a warm season turfgrass using the eddy-covariance technique. Agric. Ecosyst. Environ. 251, 11–25. https://doi.org/10.1016/j.agee.2017.09.015.

Papale, D., Reichstein, M., Aubinet, M., Canfora, E., Bernhofer, C., Kutsch, W., Longdoz,

- B., Rambal, S., Valentini, R., Vesala, T., Yakir, D., 2006. Towards a standardized processing of Net Ecosystem Exchange measured with eddy covariance technique: algorithms and uncertainty estimation. Biogeosciences 3, 571–583. https://doi.org/10.5194/bg-3-571-2006.
- Pennings, S., 2016. Monthly vegetation and invertebrate population monitoring near the Georgia Coastal Ecosystems LTER flux tower, doi: 10.6073/pasta/2eb73616b23b7b5a968c22830b4beda0.
- Reichstein, M., Falge, E., Baldocchi, D., Papale, D., Aubinet, M., Berbigier, P., Bernhofer, C., Buchmann, N., Gilmanov, T., Granier, A., Grünwald, T., Havránková, K., Ilvesniemi, H., Janous, D., Knohl, A., Laurila, T., Lohila, A., Loustau, D., Matteucci, G., Meyers, T., Miglietta, F., Ourcival, J.M., Pumpanen, J., Rambal, S., Rotenberg, E., Sanz, M., Tenhunen, J., Seufert, G., Vaccari, F., Vesala, T., Yakir, D., Valentini, R., 2005. On the separation of net ecosystem exchange into assimilation and ecosystem respiration: Review and improved algorithm. Glob. Chang. Biol. https://doi.org/10.1111/j.1365-2486.2005.001002.x.
- Richards, C.L., White, S.N., Mcguire, M.A., Franks, S.J., Donovan, L.A., Mauricio, R., 2010. Plasticity, not adaptation to salt level, explains variation along a salinity gradient in a salt marsh perennial. Estuaries and Coasts 33, 840–852. https://doi.org/10. 1007/s12337.009.9186.4
- Schedlbauer, J.L., Oberbauer, S.F., Starr, G., Jimenez, K.L., 2010. Seasonal differences in the CO2 exchange of a short-hydroperiod Florida Everglades marsh. Agri. Forest Meteorol. 150, 994–1006. https://doi.org/10.1016/j.agrformet.2010.03.005.
- Tong, C., Huang, J.F., Hu, Z.Q., Jin, Y.F., 2013. Diurnal variations of carbon dioxide, methane, and nitrous oxide vertical fluxes in a subtropical estuarine marsh on neap and spring tide days. Estuaries and Coasts 36, 633–642. https://doi.org/10.1007/ s12237-013-9596-1.
- Tweedley, J., Warwick, R., Potter, I., 2016. The contrasting ecology of temperate

- macrotidal and microtidal estuaries. In: Hughes, R.N., Hughes, D.J., Smith, I.P., Dale, A.C. (Eds.), Oceanography and Marine Biology: An Annual Review, pp. 73–171. https://doi.org/10.1201/9781315368597-3.
- US EPA, 2016. Climate change indicators: U.S. and global temperature [www document].

 United States Environ. Prot. Agency URL. https://www.epa.gov/climate-indicators/climate-change-indicators-us-and-global-temperature accessed 9.9.18.
- Vickers, D., Mahrt, L., 1997. Quality control and flux sampling problems for tower and aircraft data. J. Atmos. Ocean. Technol. 14, 512–526.
- Wang, S.R., Di Iorio, D., Cai, W.J., Hopkinson, C.S., 2018. Inorganic carbon and oxygen dynamics in a marsh-dominated estuary. Limnol. Oceanogr. 63, 47–71. https://doi. org/10.1002/lno.10614.
- Wieski, K., Pennings, S.C., 2013. Climate drivers of Spartina alterniflora salt marsh production in Georgia, USA. Ecosystems 17, 473–484. https://doi.org/10.1007/s10021-013-9732-6.
- Wilczak, J.M., Oncley, S.P., Stage, S.A., 2001. Sonic anemometer tilt correction algorithms. Boundary-Layer Meteorol 99, 127–150.
- Wutzler, T., Lucas-Moffat, A., Migliavacca, M., Knauer, J., Sickel, K., Šigut, L., Menzer, O., Reichstein, M., 2018. Basic and extensible post-processing of eddy covariance flux data with REddyProc. Biogeosciences 15, 5015–5030. https://doi.org/10.5194/bg-15-5015-2018.
- Yamamoto, A., Hirota, M., Suzuki, S., Oe, Y., Zhang, P., Mariko, S., 2009. Effects of tidal fluctuations on CO_2 and CH_4 fluxes in the littoral zone of a brackish-water lake. Limnology 10, 229–237. https://doi.org/10.1007/s10201-009-0284-6.
- Zhao, J., Malone, S.L., Oberbauer, S.F., Olivas, P.C., Schedlbauer, J.L., Staudhammer, C.L., Starr, G., 2019. Intensified inundation shifts a freshwater wetland from a CO₂ sink to a source. Global Change Biology 25, 3319–3333. https://doi.org/10.1111/gcb.14718.